INCLUSIVE PRODUCTION OF LOW-MOMENTUM CHARGED PIONS, KAONS, AND PROTONS AT x = 0 AT THE CERN INTERSECTING STORAGE RINGS

K. Guettler, B.G. Duff, M.N. Prentice, S.J. Sharrock
University College London, United Kingdom

M.W. Gibson
Bristol University, Bristol, United Kingdom

A. Duane[1], H. Newman[2], H. Ogren[3]
CERN, Geneva, Switzerland

H. Bøggild
Niels Bohr Institute, Copenhagen, Denmark

S. Henning, G. Jarlskog[4]
Lund University, Lund, Sweden

R. Little[5], T. Sanford[6], Sau Lan Wu
Massachusetts Institute of Technology, Cambridge, USA

(British-Scandinavian-MIT Collaboration)

Geneva - 18 August 1976

(Submitted to Nuclear Physics B)

---

1) Present address: Imperial College London, London, United Kingdom.
2) Present address: Harvard University, Cambridge, USA.
3) Present address: Indiana University, Bloomington, USA.
4) and CERN, Geneva, Switzerland.
5) Present address: Princeton University, Princeton, USA.
6) Present address: New York University, New York, USA.

ABSTRACT

The inclusive production of low-momentum charged pions, kaons, and protons has been measured at x = 0 over the ISR energy range $23 < \sqrt{s} < 63$ GeV. The average increase in the invariant differential cross-section is 36 ± 2% for π^+, 41 ± 2% for π^-, 52 ± 8% for K^+, 69 ± 8% for K^-, 8 ± 5% for p, and 84 ± 6% for $\bar{p}$. Pions have been measured in the range $0.04 < p_T < 0.4$ GeV/c, kaons over $0.1 < p_T < 0.3$ GeV/c, and nucleons over $0.1 < p_T < 0.5$ GeV/c.

1. INTRODUCTION

Inclusive single-particle spectra of charged hadrons have been measured at the CERN intersecting storage rings (ISR) at 90° in the centre of mass (x = 0) for particles produced with low transverse momenta over the c.m. energy range $\sqrt{s}$ = 23 GeV to $\sqrt{s}$ = 63 GeV. The transverse momentum ranges covered are $0.04 < p_T < 0.4$ GeV/c for pions, $0.1 < p_T < 0.3$ GeV/c for kaons, and $0.1 < p_T < 0.5$ GeV/c for protons. The present investigation was made in order to explore a region of low transverse momenta which was not reached by previous experiments[1,2], and to provide normalizations as accurate as the measurements of the total proton-proton cross-section[3,4]. The pion data have already been published elsewhere[5].

The measurements are estimated to have an absolute normalization uncertainty of less than 2% for pions and less than 4% for kaons and protons, and hence allow the s- and p_T-dependence of the data to be studied in detail. The increase in the pion invariant differential cross-section with s between the extremes of the ISR energy range is 36 ± 2% for π^+ and 41 ± 2% for π^-, indicating that Feynman scaling is not valid in the central region at these energies. The p_T-dependence was found to be well described by an exponential in the transverse energy.

Details of the apparatus and experimental procedure are given in Section 2, and the data analysis and reduction are described in Section 3. Finally, in Section 4 the data are discussed and compared with the results from other experiments.

2. EXPERIMENTAL DESCRIPTION

2.1 General

The data were taken with a spectrometer installed at 90° to the intersecting beams. The hodoscopes of the Pisa-Stony Brook (PSB) total cross-section experiment[3] were used as a luminosity monitor for the data normalization.

The equipment was designed to detect particles of low transverse momenta. The amount of material traversed by a triggering particle was ~ 0.6 g cm^{-2}, including the 0.18 mm thick stainless-steel vacuum pipe. The spectrometer was

situated on the inside of the interaction region so that the c.m. velocity was directed towards the equipment.

Particle identification was based on time-of-flight measurements over a flight path of 1.8 m, combined with momentum determination from deflection of the particle by a magnetic field.

2.2 The spectrometer

A schematic view of the spectrometer is presented in fig. 1, and its relation to the Pisa-Stony Brook experiment is shown in fig. 2.

The spectrometer consisted of a common front segment followed by a bending magnet which deflected particles into either an up or a down arm.

Bending in the vertical plane minimized the effect of background, which is mainly localized in the horizontal beam plane, and reduced the required dimensions of the detector as the interaction region has a small vertical height. The solid angle defined by the magnet aperture was 25 msr. The scintillation counters were used for triggering, and for time-of-flight, pulse height, and range measurements. The multiwire proportional chambers (MWPC) provided the positional data for momentum determination.

Data were collected in three modes:

1) Low-momentum pion trigger defined by the coincidence SC1·SC2·(SC3+SC6), at a magnet current setting of 60 A. These data were taken during Terwilliger (TW) runs only (see below).

2) High-momentum trigger with the magnet at the full excitation current of 180 A. The greater magnetic deflection increased the acceptance for kaons and protons, through a higher cut-off in p_T in the pion acceptance.

3) Beta-cut trigger at 180 A magnet current. The timing between counters SC1·SC2 and SC3, SC6 was adjusted so as to reject particles with a velocity $\beta > 0.85$. This cut enhanced the fraction of kaons and protons in the trigger.

In fig. 3 the p-β scatter plots show the relative merits of these different triggers.

The proportional chambers had three wire planes, each with a gap of ±6 mm. Horizontal, vertical, and diagonal (45°) wires were spaced 2 mm, 4 mm, and 4 mm, respectively. The dimensions of the front chambers 1-3 were 250 × 120 × 90 mm^3, and the back chambers 5 and 6 measured 300 × 300 × 90 mm^3. Chamber 4 covered the entire magnet exit aperture and was 500 × 290 × 90 mm^3 in size. The total system contained 1576 wires. The operating gas was pure argon bubbled through methylal at 0°C. The plane efficiencies defined as the probability of obtaining a hit on one plane, given a signal on the other two planes of the modules, were > 99%.

The front trigger counter measured 30 × 6 × 2 mm^3 and had phototubes SC1 and SC2 attached at either end. Two sets of back counters, SC3-SC5 and SC6-SC8, were installed behind the up and down chambers. They consisted of a 50 mm thick total energy counter sandwiched between two 5 mm thick dE/dx counters. The outer dimensions of SC3-SC8 were 340 × 400 mm^2 and covered more than the chamber apertures. Only the first of the three counters was required in the trigger. All the counters were mapped in a test beam at the CERN Proton Synchrotron (PS) and gave typical TOF resolutions of 1.0 nsec FWHM for minimum ionizing particles.

The bending magnet had a useful aperture of 230 × 286 mm^2 and a field length of 540 mm. The maximum field integral was 1.83 kGm at 180 A current. The uncertainty in the field calibration produced an error on the momentum resolution $\Delta p/p$ of ±0.7%.

2.3 Luminosity monitor

The ISR luminosity was monitored using two separate coincidences of the PSB hodoscope system. The two monitors H34 and B12 (see fig. 2) were sensitive to cross-sections of 25 mb and 0.8 mb, respectively. Their counting rates were recorded continuously throughout the data taking, gated by the live time of the spectrometer. The luminosity monitors were calibrated frequently in special luminosity runs using the van der Meer method of vertical separation of the ISR beams. The luminosity monitors gave cross-section values consistent to within 2% for each ISR run. Cross-sections at the same energy from different ISR runs showed fluctuations of up to 3%, mainly due to changes in background conditions and beam position.

However, the very accurate luminosity determination applies only to the data obtained during the special TW runs. During ordinary non-TW runs the luminosity was recorded but no monitor calibration was carried out.

2.4 Data collection

The data acquisition was controlled by a PDP-8 computer with 8 K memory. The data were read in through a CAMAC system consisting of TDC and ADC scalers for TOF and PHT measurements, parallel input registers for bit patterns, and scalers for monitor rates. The MWPC read-out required a purpose-built CAMAC interface.

The bulk of the data were collected during ISR runs in which the horizontal width of the interaction region was reduced to about 6 cm (Terwilliger runs) Figure 4 shows the size of the interaction region for such beams. At the beginning of a run the luminosity monitors were calibrated. Then a data run with zero magnet current was taken to determine the chamber alignment.

Data were taken in pairs of runs with opposite magnet polarity to minimize apparatus asymmetries. Some pion runs at 180 A were taken for acceptance consistency checks. The quality of the data was monitored on-line through displays of accumulated histograms and through event pictures giving also a momentum value calculated by a hardware processor[6].

Data were taken at all five nominal ISR energies, $\sqrt{s}$ = 23, 31, 45, 53, and 63 GeV. Runs with only one circulating beam allowed estimates of the background rates due to beam-gas and beam-wall interactions to be made.

The data sample reported on here consists of 10^6 events from TW runs and 2.5×10^5 events from non-TW runs.

3. DATA ANALYSIS

3.1 Event reconstruction

The chamber information was used to reconstruct tracks in the spectrometer. Coordinates from three chambers were required to give a straight line in the non-bend view, and two chambers with correlated hits were used to give front and back segments in the bend view. Good tracks were required to be within certain channel widths of any hit wires, and were accepted after cuts based on a χ^2 test from the fit in the non-bend view and on the linking of the front and back segments at the magnet centre. A maximum of 10 track candidates was allowed for a given trigger.

A momentum value was calculated using the entrance and exit points to the magnetic field and a grid of field integral values derived from a detailed field map. The TOF was determined using the mean of the SC1, SC2 and of the first back counter (SC3 or SC6) readings. All TOF readings were corrected for transit time and pulse-height variations in the counter.

In a second analysis pass, the reconstructed events were analysed with tight geometrical cuts on all physical apertures of the spectrometer. The number of accepted events in the up or the down arm was found to be very sensitive to the vertical position of the interaction region. All the aperture cuts were therefore aligned with the centre of the interaction region in the vertical and horizontal directions. Further cuts of the form $A + B/p\beta$ were imposed on velocity-dependent parameters such as χ^2 and the linking quantities. After these geometry cuts, the remaining events were identified by their mass as derived from the momentum and the measured TOF. Upper momentum limits on a clean particle separation were determined by inspection of the experimental p-β plots (fig. 3).

Multiple candidates formed only a small fraction of less than 1% of the final data sample. Each such track candidate was projected through all the cuts, and the first good candidate was accepted. This procedure did not introduce any bias

into any of the experimental distributions. Chamber efficiencies and monitor rates were checked for every 1000 events.

The reconstruction program found track candidates for typically 60% of the initial triggers, and the final data sample of identified events contained about 15% of the triggers, the reduction being mainly due to geometry cuts.

3.2 Monte Carlo simulation

The momentum acceptance was calculated using a Monte Carlo (MC) program. Experimental source distributions were used to generate particles at the interaction diamond. The propagation through the spectrometer took into account multiple scattering, energy loss, nuclear interactions, and particle decays. Particle momenta were calculated using a detailed field map with entries. The momentum resolution is shown in fig. 5. The acceptance was determined as the ratio of accepted to thrown events for a given bin in p_T. The MC data were generated with an exponential p_T spectrum and were subsequently reconstructed and analysed using the same programs as the data. The acceptance was found to be insensitive to variations in the generated spectrum; in particular, an acceptance generated with an exp $(-B\mu_T)$ spectrum yielded the same cross-section values. Variations of ±10% in the geometrical cuts did not affect the cross-sections.

MC pion acceptances were generated for TW runs only, at 60 A and 180 A (fig. 6a). Kaon and proton acceptances were required for both TW and non-TW runs at 180 A (fig. 6b). The investigation of the data source distributions revealed no s-dependence of the diamond width and centre position. As all the data cuts had been symmetrized about the diamond centre, only one MC acceptance with a source centred on the spectrometer axis was needed for all energies. The background contamination was estimated using MC events generated with a uniform source distribution.

No analytical smoothing of the acceptance was done. Events were generated in 0.01 GeV/c bins up to p_T = 0.3 GeV/c and in 0.025 GeV/c bins above 0.3 GeV/c. The calculated cross-sections have been rebinned into 0.02 or 0.04 GeV/c bins below a p_T of 0.3 GeV/c to account for the finite MC statistics.

The correction for nuclear interaction for all particles was less than 5% at all values of p_T. Any contamination due to misidentified particles, mainly due to decays, was estimated from the appropriate MC data. The contamination in the pion spectra due to charged kaons was found to be less than 1%. The pion and proton contamination in the kaon spectra was estimated to be completely negligible. The proton data are free of any such contaminations.

3.3 Corrections

A background subtraction has been applied to the pion data only.

The tails of the diamond distributions were extrapolated over the entire source region and subtracted from the appropriate p_T spectrum. This correction was much less than 1% for all TW runs and all particle types except protons, and independent of energy. The kaon and proton data are a mixture of TW runs and non-TW runs, for which it was not possible to evaluate the background since the spectrometer aperture did not cover the full extent of the interaction region. However, since the luminosity in non-TW runs was considerably higher than in the TW runs, it can be assumed that the non-TW background is not larger than what is observed in the TW runs. For protons this TW background is of the order of 8% at 150 MeV/c, decreasing to about 3% at 500 MeV/c, essentially independent of energy, but since this is a crude estimate no subtraction was actually done to the data.

For the pions two important sources of background were considered, as discussed in ref. 5: electron contamination from photon conversions and Dalitz decay, and pion background from the decay of K^0_S. As can be seen in fig. 3, electrons and pions were clearly separated by TOF and momentum measurements below 0.12 GeV/c. At higher momenta a correction based on the calculated electron to pion ratio was used, as shown in fig. 7. The ratio of pions coming from the decay $K^0_S \to \pi^+\pi^-$ to all pions was calculated and is shown in fig. 8, but no correction for this was applied to the data.

A proton from a Λ decay is normally accepted within the cuts, but no corrections due to $\Lambda\bar{\Lambda}$ production have been applied to the proton or antiproton cross-sections. The Λ production cross-section has been measured at the ISR for $p_T >$ > 0.6 GeV/c, but its energy dependence has not been investigated[7].

3.4 Data merging and errors

The data were accumulated and analysed in runs of $\sim$ 60,000 events. Particle spectra for an equal number of such positive and negative polarity runs were summed for each ISR run. The summed spectra were combined with the appropriate MC acceptance to give cross-sections. The TW run cross-sections at each ISR energy were added after weighting according to the total luminosities. The kaon and proton data include also contributions from non-TW runs in order to increase the statistics. The p_T shape of the non-TW data was found to be equal to the TW data, and the spectra were combined after a renormalization of the integrated cross-sections to the TW data. An additional renormalization error of 4% was added in quadrature to the non-TW data.

The internal consistency between runs within one ISR run was checked by comparing the pion cross-sections in the range 0.1-0.3 GeV/c. This comparison yielded an estimate of the run-to-run uncertainties of 2%. Good agreement was found between data from the up and down arms obtained with opposite magnet polarities, and

between data obtained with the two magnet currents. The errors on the data are the combined experimental and MC statistical errors only. The errors on the lowest p_T bin for kaons and protons have been increased by 10% to take account of increased acceptance uncertainties. In this p_T interval, $0.10 < p_T < 0.14$ GeV/c, the acceptance decreases from 50% to 20% of its maximum value for kaons, and from 100% to 65% for protons.

By comparing the run-to-run fluctuation in the luminosity measurement, the absolute normalization of the pion data is estimated to be about 2%. Owing to the combination of TW and non-TW data, the kaon and proton spectra are only accurate to within ±4%.

4. RESULTS AND CONCLUSIONS

Invariant single inclusive cross-sections for pions are given in ref. 5. The results for kaons and protons are shown in figs. 9 and 10 and are listed in table 1. For comparison the data of Alper et al.[1] below $p_T = 0.6$ GeV/c are also shown in figs. 9 and 10. The invariant differential distributions have been fitted to the following forms:

$$As^{\alpha} e^{Bp_T}$$

$$As^{\alpha} e^{Bp_T^2}$$

$$As^{\alpha} e^{B\mu_T} ,$$

where $\mu_T = \sqrt{m^2 + p_T^2}$ is the transverse energy of the particle. The results of the fits are given in table 2. The increase with s of the differential cross-section over the ISR energy range 23-63 GeV is on the average 52 ± 8% for K^+, 69 ± 8% for K^-, 8 ± 5% for p, and 84 ± 6% for $\bar{p}$. This can be compared to an increase of 36 ± 2% and 41 ± 2% for π^+ and π^-.

It should be noted that for all particle types there is some p_T-dependence in the s-dependence of the differential cross-sections (fig. 11). There is a more pronounced increase with energy in the differential cross-section at higher p_T. However, the very low p_T pion cross-sections seem to increase more at small values of p_T ($p_T < 0.1$ GeV/c) rather than at intermediate p_T ($0.1 < p_T < 0.4$ GeV/c) [5].

Fits to the p_T-dependence indicate that a linear exponential in the transverse energy is appropriate for pions. An exponential in p_T (or p_T^2) cannot reproduce the turnover found at very low p_T. For kaons, the p_T range of the data is too limited and cannot distinguish between an exponential in p_T or in μ_T. When measurements

at higher p_T (ref. 1) (up to 0.6 GeV/c) are also included, a turnover becomes apparent in the combined data and the second or third fit is favoured. The proton cross-sections show no noticeable tendency to flatten off and are well described by a linear exponential in p_T. The p_T-dependence of the antiprotons is also best described by the first fit, although the exponential in transverse energy cannot be excluded. However, for $p_T > 0.6$ GeV/c neither fit seems to adequately represent the data which show the beginning of the high p_T regime.

Figure 12 shows the change in particle composition with p_T as the ISR energy is increased from $\sqrt{s}$ = 23 to 63 GeV, and as obtained from a fit to As^{α} for each p_T interval. The different particle types in this experiment overlap in p_T only from 0.1 to 0.3 GeV/c; therefore the data of Alper et al. (ref. 1) in the range $0.4 < p_T < 0.6$ GeV/c are included for comparison.

The heavier particles become more abundant at higher p_T and with increasing energy (except for protons). Figure 13 shows the variation in the ratio of particle to antiparticle with p_T and s. The strongest variation is seen in the $p/\bar{p}$ ratio, where a large fraction of protons at the lowest ISR energy (and low p_T) appear to belong to the incoming beams, whereas at larger s and p_T the detected baryons tend to be produced in equal numbers.

In order to expand the available energy range, we have compared our pion results with data taken at lower energies[8-10] (table 3). Several predictions have been given on the energy dependence of the inclusive π^+ and π^- production in the central region [cf. Narayan et al.[11]]. We have fitted the π^+ and π^- data over the range $\sqrt{s}$ = 6 to 63 GeV at a fixed p_T of 0.2 GeV/c to

$$A + B\, s^{\alpha} ,$$

$$A - B\, s^{-\alpha} ,$$

$$A + B \ln s .$$

The fits are shown in fig. 4 and the fitting parameters are given in table 4. As can be seen, all fits give an acceptable χ^2, and the data are compatible with either an asymptotically constant invariant differential cross-section for pions (of about 220 mb at p_T = 0.2 GeV/c), or an unlimited increase like ln s or s^{α} with $\alpha \sim 0.10$-0.20. It can be noticed that the negative power of s is numerically quite small, and larger values like 1/4 or 1/2 are excluded by the data.

The Feynman scaling hypothesis[12] used at x = 0 suggests no energy dependence, which is of course not consistent with the data; but, on the other hand, Feynman scaling is not necessarily exact at x = 0.

Acknowledgements

We acknowledge close collaboration with the Pisa-Stony Brook group. We would like to thank many members of the CERN ISR Division and the ISR experimental support group for much help during the preparation and running of this experiment.

The MIT group would like to acknowledge the help of U. Becker, and Professors S.C.C. Ting and M. Deutsch for their support throughout the experiment.

The experiment was supported by the Science Research Council, United Kingdom, the Research Councils in Denmark and Sweden, and the Laboratory for Nuclear Science of MIT and ERDA, USA.

REFERENCES

1) B. Alper et al., Nuclear Phys. B100 (1975) 237.

2) M. Banner et al., Phys. Letters 41B (1972) 547.

3) U. Amaldi et al., Phys. Letters 44B (1973) 112.

4) S.R. Amendolia et al., Phys. Letters 44B (1973) 119.
S.R. Amendolia et al., Nuovo Cimento 17A (1973) 735.

5) K. Guettler et al., Inclusive production of low-momentum charged pions at x = 0 at the CERN Intersecting Storage Rings, to be published in Phys. Letters B.

6) C. Maclean and G. McPherson, Proc. 2nd Internat. Symposium on Nuclear Electronics, Ispra, 1975 (EUR-5370), p. 307.

7) F.W. Büsser et al., Phys. Letters 61B (1976) 309.

8) V. Blobel et al., DESY 73-36 (1973) and Phys. Letters 39B (1972) 303.

9) C. Bromberg et al., preprint UR-563 (1976).

10) Y. Cho et al., Phys. Rev. Letters 31 (1973) 413.

11) D.S. Narayan, Nuovo Cimento Letters 2, No. 19 (1971) 975 and Nuclear Phys. B34 (1971) 386.
Chan Hong-Mo et al., Phys. Letters 40B (1972) 406.

12) R.P. Feynman, Phys. Rev. Letters 23 (1969) 1415.

Table 1

Invariant differential cross-sections of inclusive production of $K^{\pm}$, p, and $\bar{p}$ ($mb/GeV^2/c^3$)

	p_T (GeV/c)	$\sqrt{s}$ (GeV)				
		23	31	45	53	63
K^+	0.123	3.86 ± 0.61	3.40 ± 0.43	3.88 ± 0.59	4.54 ± 0.42	3.46 ± 0.64
	0.161	3.44 ± 0.35	3.28 ± 0.25	3.60 ± 0.31	4.34 ± 0.27	4.43 ± 0.36
	0.200	2.66 ± 0.21	2.81 ± 0.17	3.18 ± 0.23	3.92 ± 0.21	3.67 ± 0.24
	0.240	2.54 ± 0.23	2.50 ± 0.13	2.90 ± 0.19	3.39 ± 0.16	3.44 ± 0.18
	0.280	2.10 ± 0.17	2.20 ± 0.12	2.73 ± 0.17	2.96 ± 0.14	3.44 ± 0.16
K^-	0.123	2.58 ± 0.44	3.09 ± 0.41	3.57 ± 0.54	4.34 ± 0.43	3.99 ± 0.68
	0.161	2.26 ± 0.29	2.88 ± 0.23	3.25 ± 0.30	3.59 ± 0.24	3.82 ± 0.34
	0.200	2.20 ± 0.21	2.50 ± 0.16	2.95 ± 0.23	3.41 ± 0.19	2.82 ± 0.21
	0.240	1.84 ± 0.15	2.07 ± 0.12	2.67 ± 0.18	2.96 ± 0.15	3.18 ± 0.18
	0.280	1.68 ± 0.14	1.76 ± 0.10	2.32 ± 0.15	2.58 ± 0.12	3.05 ± 0.16
p	0.123	3.51 ± 0.33	2.81 ± 0.18	2.82 ± 0.23	3.05 ± 0.18	3.61 ± 0.25
	0.161	2.92 ± 0.20	2.68 ± 0.13	2.65 ± 0.15	2.84 ± 0.13	2.69 ± 0.14
	0.200	2.49 ± 0.18	2.30 ± 0.11	2.36 ± 0.13	2.56 ± 0.11	2.25 ± 0.10
	0.240	2.32 ± 0.16	1.99 ± 0.09	2.05 ± 0.11	2.27 ± 0.10	2.17 ± 0.09
	0.280	2.00 ± 0.14	1.78 ± 0.08	1.85 ± 0.10	2.03 ± 0.09	1.94 ± 0.08
	0.325	1.65 ± 0.13	1.52 ± 0.08	1.68 ± 0.10	1.83 ± 0.09	1.77 ± 0.09
	0.375	1.42 ± 0.11	1.37 ± 0.07	1.48 ± 0.09	1.61 ± 0.08	1.56 ± 0.08
	0.424	1.22 ± 0.09	1.22 ± 0.07	1.26 ± 0.08	1.31 ± 0.07	1.32 ± 0.09
	0.474	1.06 ± 0.09	1.05 ± 0.06	1.06 ± 0.08	1.12 ± 0.06	1.28 ± 0.09
$\bar{p}$	0.123	0.93 ± 0.12	1.34 ± 0.12	1.45 ± 0.15	1.81 ± 0.13	1.72 ± 0.18
	0.161	0.87 ± 0.09	1.14 ± 0.07	1.35 ± 0.10	1.59 ± 0.08	1.43 ± 0.10
	0.200	0.88 ± 0.08	1.06 ± 0.06	1.27 ± 0.09	1.52 ± 0.08	1.48 ± 0.09
	0.240	0.80 ± 0.07	0.91 ± 0.05	1.14 ± 0.07	1.34 ± 0.07	1.40 ± 0.08
	0.280	0.69 ± 0.06	0.78 ± 0.04	1.00 ± 0.06	1.20 ± 0.06	1.18 ± 0.06
	0.325	0.63 ± 0.06	0.78 ± 0.05	0.94 ± 0.07	1.09 ± 0.06	1.01 ± 0.07
	0.375	0.55 ± 0.06	0.68 ± 0.04	0.82 ± 0.06	0.98 ± 0.05	1.06 ± 0.07
	0.424	0.46 ± 0.05	0.56 ± 0.04	0.70 ± 0.06	0.84 ± 0.05	1.09 ± 0.08
	0.474	0.40 ± 0.04	0.44 ± 0.03	0.65 ± 0.06	0.72 ± 0.05	0.92 ± 0.07

Table 2

Fits to the invariant differential cross-sections of $K^{\pm}$, p, and $\bar{p}$ at x = 0 over the range 0.1-0.3 GeV/c for the kaons and 0.1-0.5 GeV/c for the nucleons and $23 < \sqrt{s} < 63$ GeV. Errors correspond to a change in χ^2 by 1 unit.

Fit		A	α	B	χ^2/NDF
$As^{\alpha} e^{Bp_T}$	K^+	1.14 ± 0.01	0.213 ± 0.006	-2.64 ± 0.21	21/22
	K^-	0.692 ± 0.010	0.265 ± 0.002	-2.85 ± 0.06	20/22
	p	3.21 ± 0.03	0.038 ± 0.001	-2.85 ± 0.03	43/42
	$\bar{p}$	0.195 ± 0.002	0.310 ± 0.001	-2.49 ± 0.03	43/42
$As^{\alpha} e^{Bp_T^2}$	K^+	0.889 ± 0.021	0.210 ± 0.002	-6.12 ± 0.67	22/22
	K^-	0.517 ± 0.041	0.264 ± 0.010	-6.50 ± 0.68	22/22
	p	2.18 ± 0.02	0.037 ± 0.001	-4.61 ± 0.07	84/42
	$\bar{p}$	0.141 ± 0.001	0.306 ± 0.001	-4.03 ± 0.06	56/42
$As^{\alpha} e^{B\mu_T}$	K^+	23.9 ± 0.3	0.212 ± 0.002	-6.66 ± 0.02	22/22
	K^-	17.4 ± 0.2	0.264 ± 0.002	-7.09 ± 0.03	22/22
	p	13 080 ± 110	0.035 ± 0.001	-9.24 ± 0.01	79/42
	$\bar{p}$	284 ± 94	0.307 ± 0.015	-8.09 ± 0.25	53/42

Table 3

Compilation of invariant differential cross-sections for the inclusive production of π^+ and π^- at x = 0 and p_T = 0.2 GeV/c. The assigned errors include our estimated uncertainty in normalization.

$\sqrt{s}$ (GeV)	π^+	π^-	Normalization uncertainty (%)	Ref.
4.93	31.3 ± 1.0	17.7 ± 0.6	3	7a
6.84	34.6 ± 1.2	22.6 ± 0.8	3	7a
13.8		31.5 ± 2.5	5	7b
19.6	39.5 ± 3.6	39.0 ± 2.8	5	7c
23.4	45.2 ± 7.2	45.0 ± 7.1	15	1
23.4	45.9 ± 1.3	43.0 ± 1.3	2	*
27.4		43.0 ± 3.3	5	7c
31	50.9 ± 5.4	51.7 ± 5.5	10	1
31	49.8 ± 1.5	46.4 ± 1.4	2	*
45	54.9 ± 4.3	51.6 ± 4.0	6	1
45	54.8 ± 1.6	53.3 ± 1.6	2	*
53	53.8 ± 3.8	52.9 ± 3.7	6	1
53	58.7 ± 1.8	56.9 ± 1.8	2	*
63	67.9 ± 7.6	66.0 ± 7.5	10	1
63	61.3 ± 1.7	61.3 ± 1.8	2	*

* This experiment.

Table 4

Parameters of the fits to the over-all s-dependence of invariant differential cross-sections for π^+ and π^- at p_T = 0.2 GeV/c and x = 0 (the data points are given in table 3).

	Particle	A	B	α	χ^2/NDF
$A + B\, s^{\alpha}$	π^+	17.2 ± 2.9	+7.2 ± 2.0	0.22 ± 0.03	4/10
	π^-	-5.9 ± 1.3	+58 ± 12	0.087 ± 0.012	5/12
$A - B\, s^{-\alpha}$	π^+	233 ± 33	222 ± 33	0.029 ± 0.006	14/10
	π^-	215 ± 32	229 ± 31	0.045 ± 0.009	11/12
$A + B \ln s$	π^+	13.1 ± 1.5	5.5 ± 0.3		12/11
	π^-	-8.7 ± 1.0	8.2 ± 0.2		7/13

Figure captions

Fig. 1 : View of the experimental apparatus. CH1-6 are multiwire proportional chambers, SC1-8 are scintillation counters.

Fig. 2 : Schematic layout of the Pisa-Stony Brook experimental apparatus (ref. 2). The counter hodoscopes H3, H4 and H4Θ were used to monitor the luminosity. The small B12 luminosity counters are located in the region of the H3 and H4 hodoscopes.

Fig. 3 : Momentum-beta scatter plots illustrating the particle separation in the three different modes of data taking; for a magnet current of 60 A, 180 A, and 180 A and β-cut.

Fig. 4 : Source distribution of events for a TW run in the low p_T magnet setting.

Fig. 5 : Momentum resolution for pions in the low p_T magnet setting.

Fig. 6 : a) Pion acceptances for TW runs in the low p_T and high p_T magnet settings.
: b) Kaon and proton acceptances for TW runs in the high p_T magnet setting.

Fig. 7 : Electron-to-pion ratio as a function of the transverse laboratory momentum. The solid line is the calculated ratio $R(e/\pi)$, which falls about 10% below the data points. The dashed line represents the correction actually applied to the data, $R = 0.001\ p_{lab}^{-2.11}$.

Fig. 8 : Percentage contamination of pions from K_S^0 decay.

Fig. 9 : Invariant differential K^+, K^-, p, and $\bar{p}$ cross-sections at x = 0 versus the transverse momentum. The data points are from this experiment (●) and for comparison also from ref. 1 (○). The solid line represents a fit of As^{α} exp $(B\mu_T)$ to the data, and the dashed line is an extrapolation of this fit.

Fig. 10 : Invariant differential cross-sections at $\sqrt{s}$ = 45 GeV and x = 0 versus the transverse energy of positive and negative particles. The symbols (●, ■ , ▲) refer to π, K, and p from this experiment and (○ , □ , Δ) to the data of ref. 1.

Fig. 11 : The p_T-dependence of the increase with s over the ISR energy range of the K^+, K^-, p, and $\bar{p}$ invariant differential cross-sections. The cross-section ratio between $\sqrt{s}$ = 63 and 23 GeV is deduced from a fit to As^{α} at the given value of p_T.

Fig. 12 : Particle composition as a function of p_T at $\sqrt{s}$ = 23 and 63 GeV. The data points from this experiment in the p_T range of 0.1-0.3 GeV/c are compared to the data of ref. 1 over 0.4 to 0.6 GeV/c.

Fig. 13 : Particle/antiparticle ratio as a function of p_T at $\sqrt{s}$ = 23 and 63 GeV.

Fig. 14 : The s-dependence of the invariant differential cross-section of π^+ and π^- at p_T = 0.2 GeV/c and x = 0. The data (see also table 3) are taken from: (●) ref. 1, (■) ref. 8, (□) ref. 9, (Δ) ref. 10, and (○) this experiment. The values of the parameters are given in table 4.

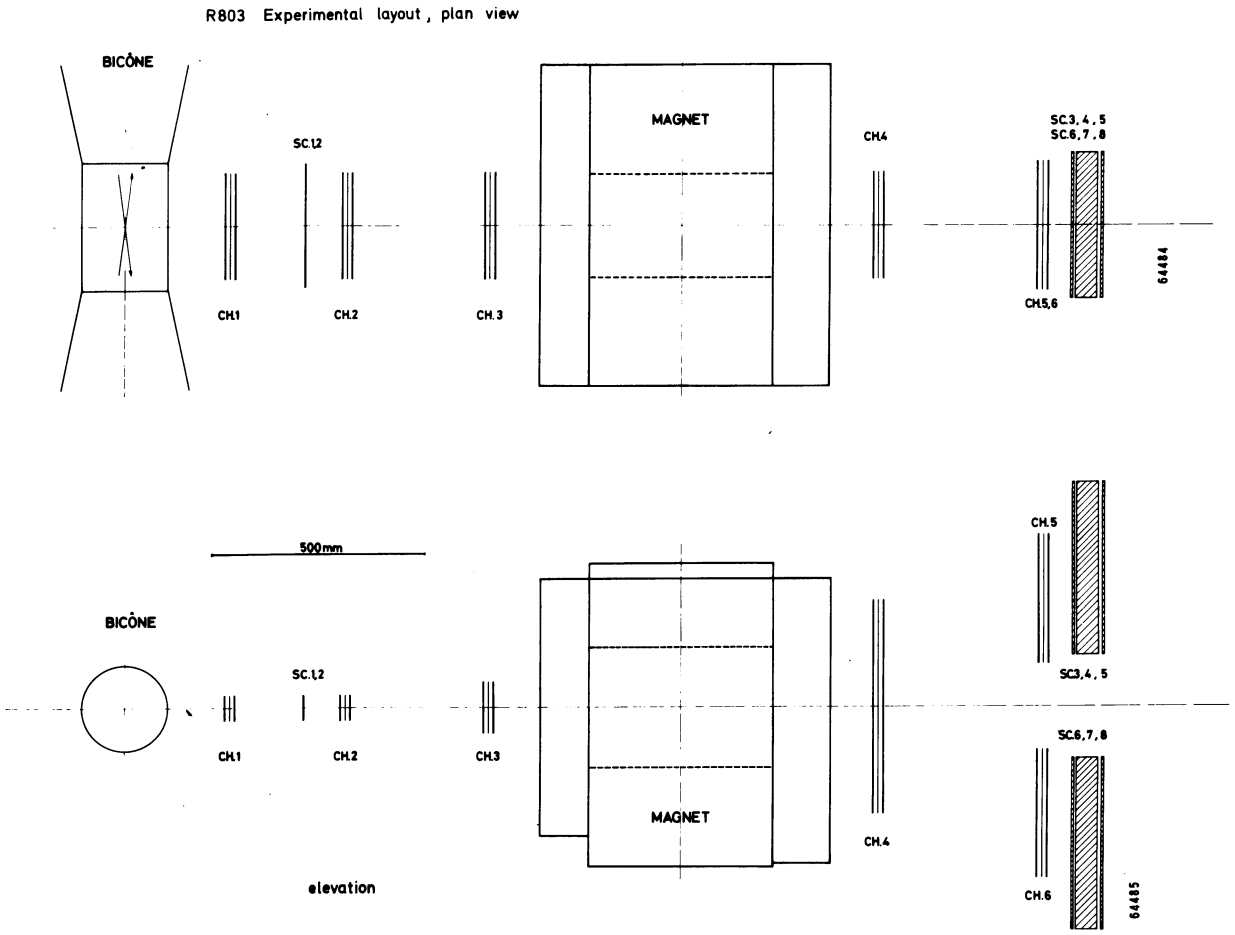
R803 Experimental layout, plan view
BICÔNE
SC.1,2
MAGNET
CH.4
SC.3,4,5
SC.6,7,8
CH.1
CH.2
CH.3
CH.5,6
64484
500mm
CH.5
BICÔNE
SC.1,2
SC3,4,5
SC6,7,8
CH.1
CH.2
CH.3
MAGNET
CH.4
CH.6
64485
elevation

Fig. 1

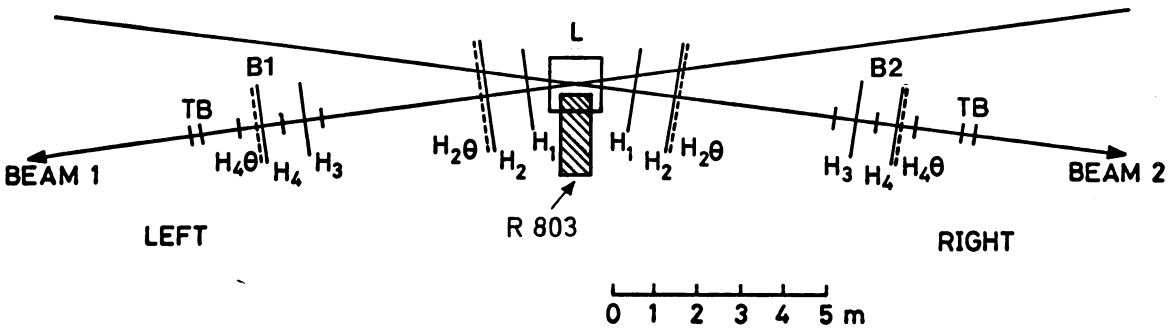
L
B1
B2
TB
TB
BEAM 1
BEAM 2
$H_4\theta$
H_4
H_3
$H_2\theta$
H_2
H_1
H_1
H_2
$H_2\theta$
H_3
H_4
$H_4\theta$
R 803
LEFT
RIGHT
0 1 2 3 4 5 m

Fig. 2

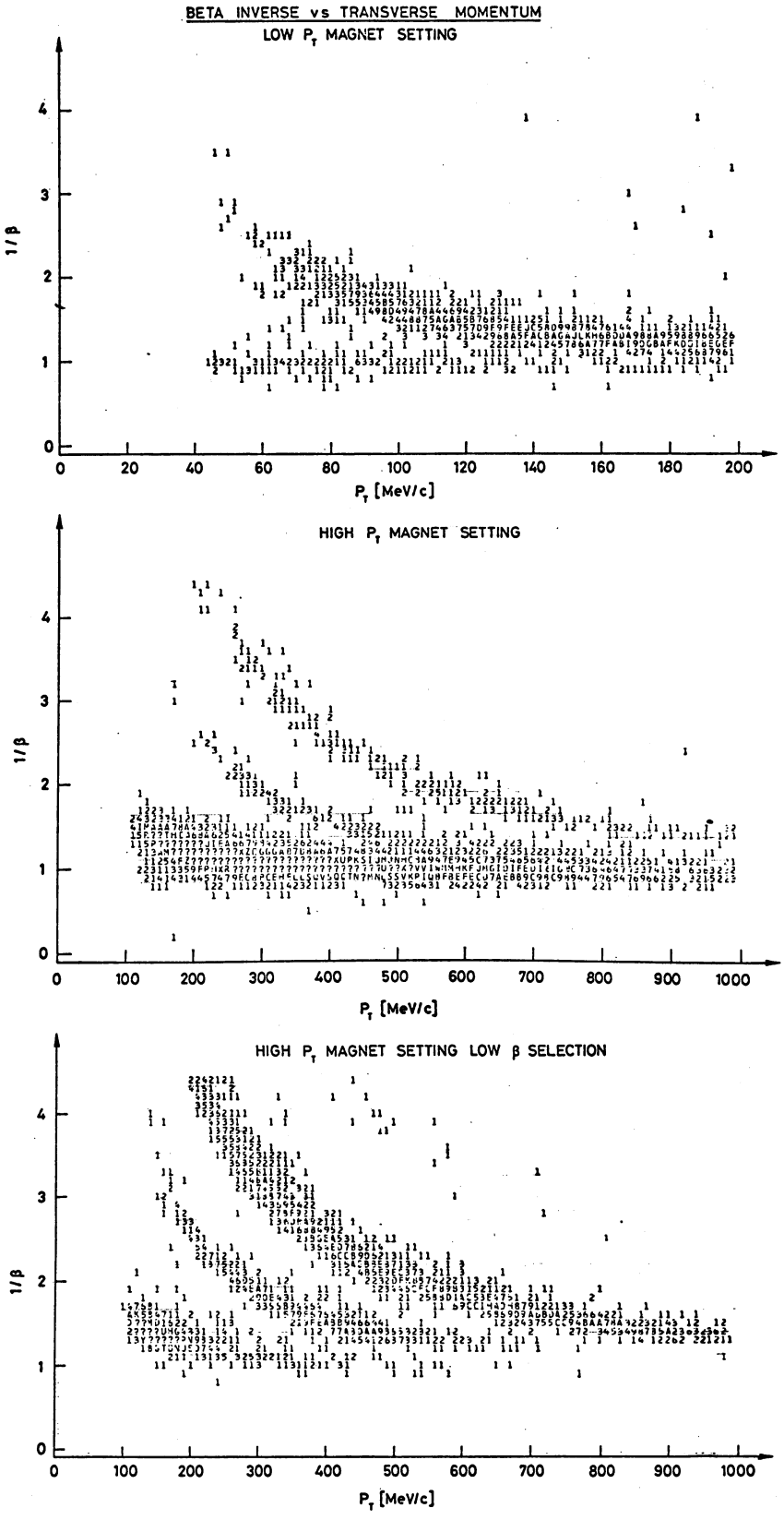
BETA INVERSE vs TRANSVERSE MOMENTUM
LOW P_T MAGNET SETTING
1/β
P_T [MeV/c]
HIGH P_T MAGNET SETTING
1/β
P_T [MeV/c]
HIGH P_T MAGNET SETTING LOW β SELECTION
1/β
P_T [MeV/c]

Fig. 3

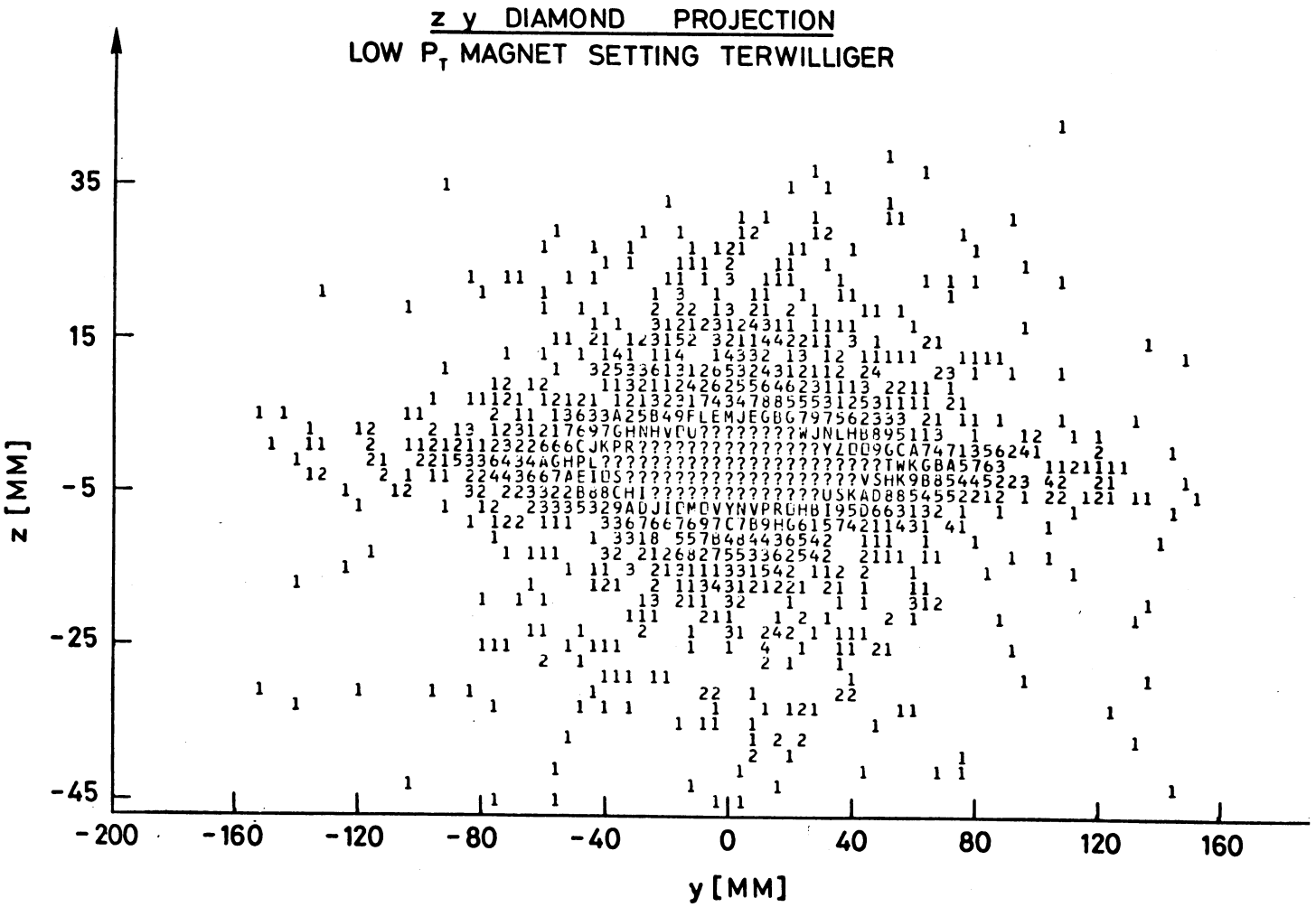
z y DIAMOND PROJECTION
LOW P_T MAGNET SETTING TERWILLIGER
z [MM]
35
15
-5
-25
-45
-200
-160
-120
-80
-40
0
40
80
120
160
y [MM]

Fig. 4

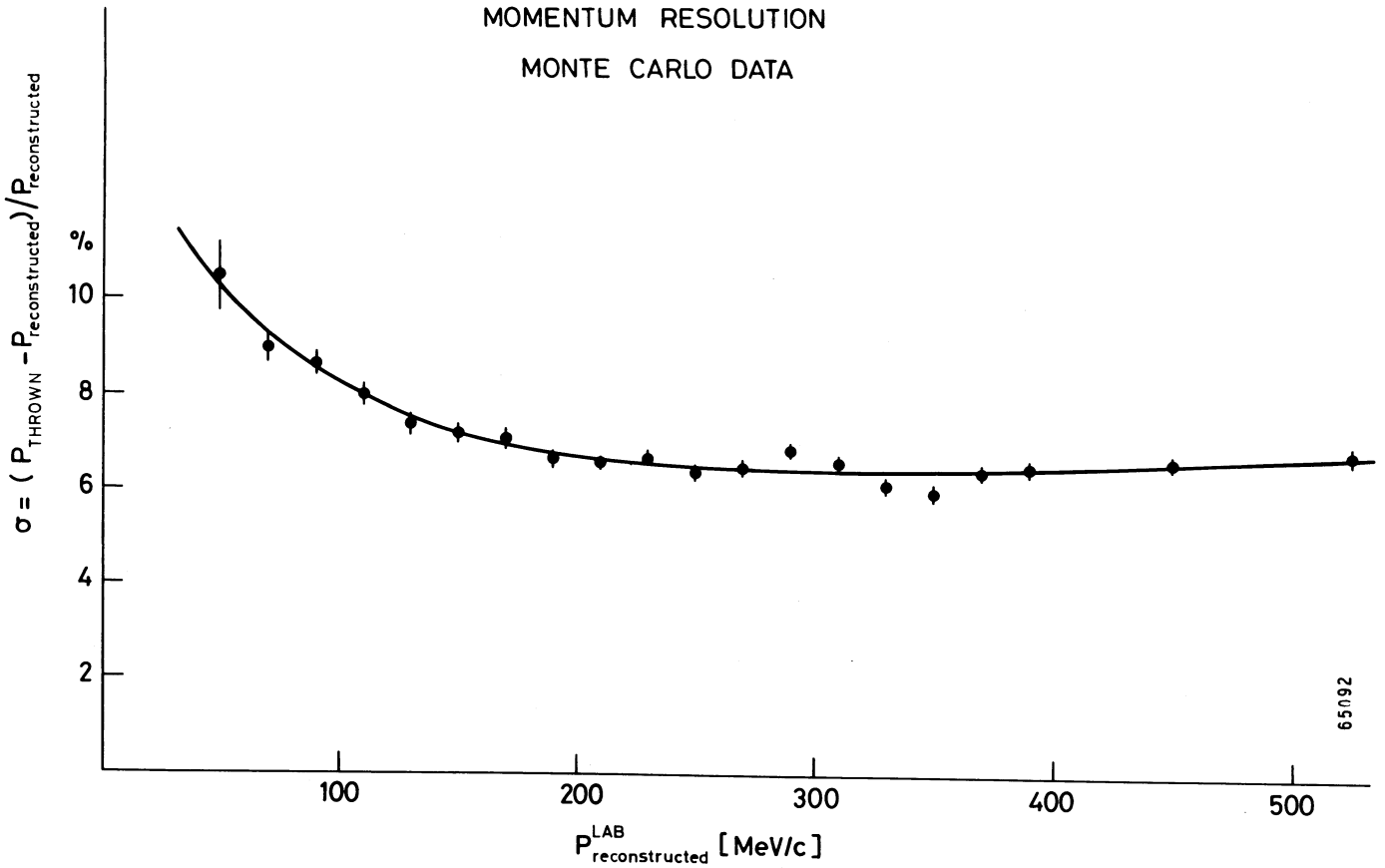
MOMENTUM RESOLUTION
MONTE CARLO DATA
σ = (P_THROWN - P_reconstructed)/P_reconstructed
%
10
8
6
4
2
100
200
300
400
500
P^LAB_reconstructed [MeV/c]
65092

Fig. 5

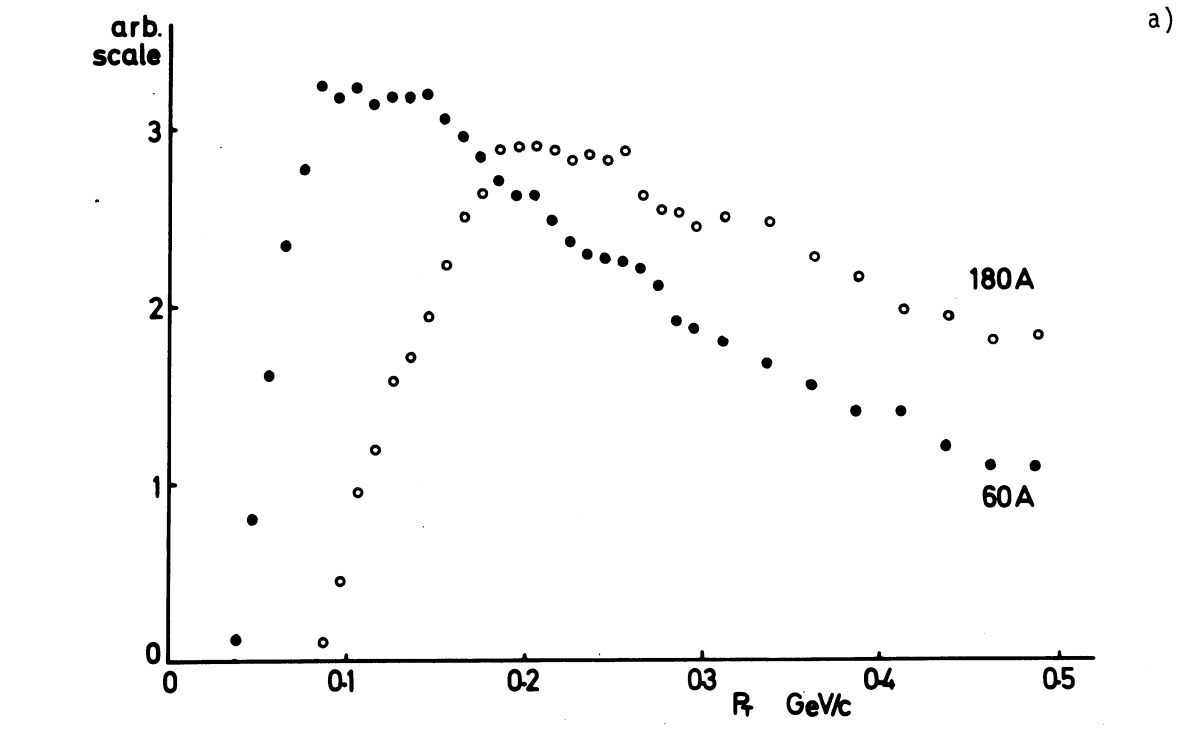
a)
arb.
scale
3
2
1
0
180A
60A
0
0·1
0·2
0·3
0·4
0·5
P_T GeV/c

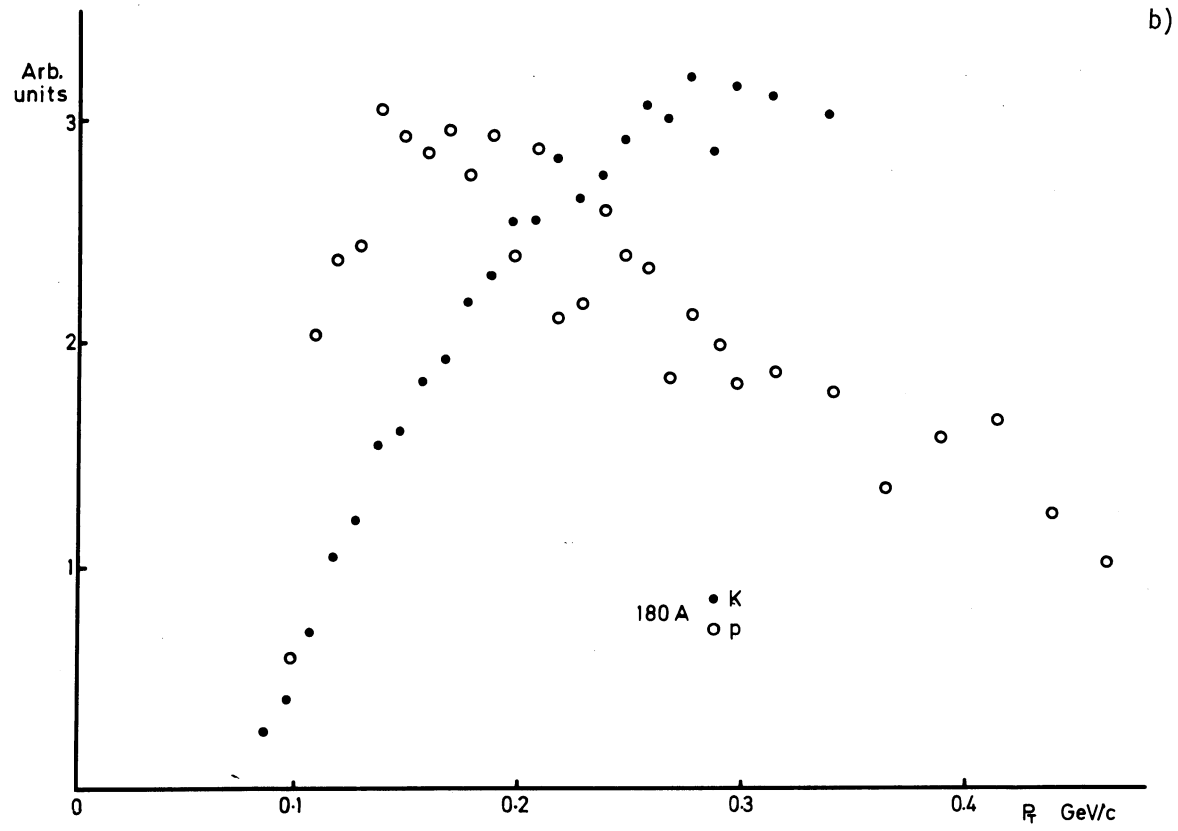
b)
Arb.
units
3
2
1
0
180 A
K
p
0·1
0·2
0·3
0·4
P_T GeV/c

Fig. 6

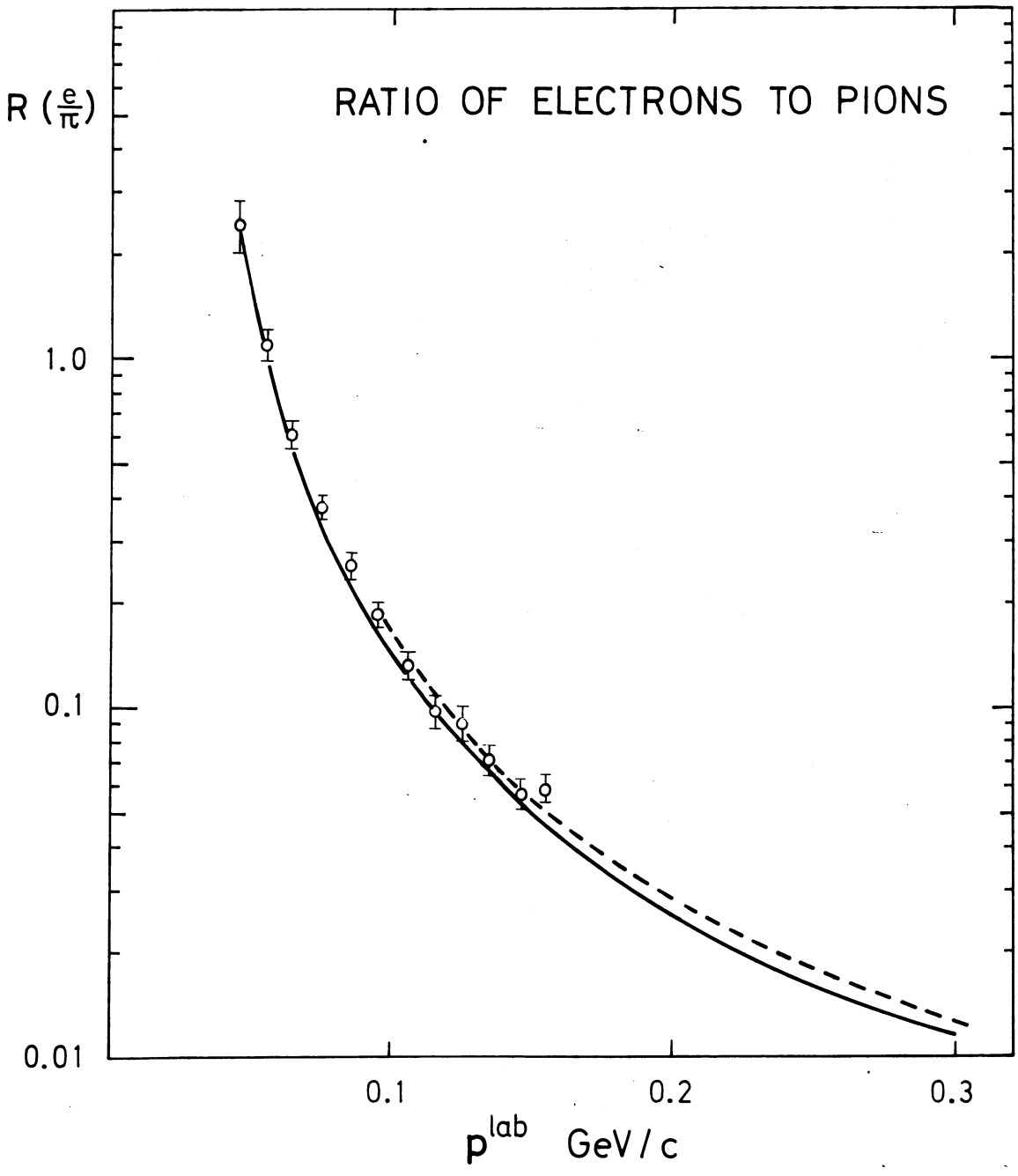

Fig. 7

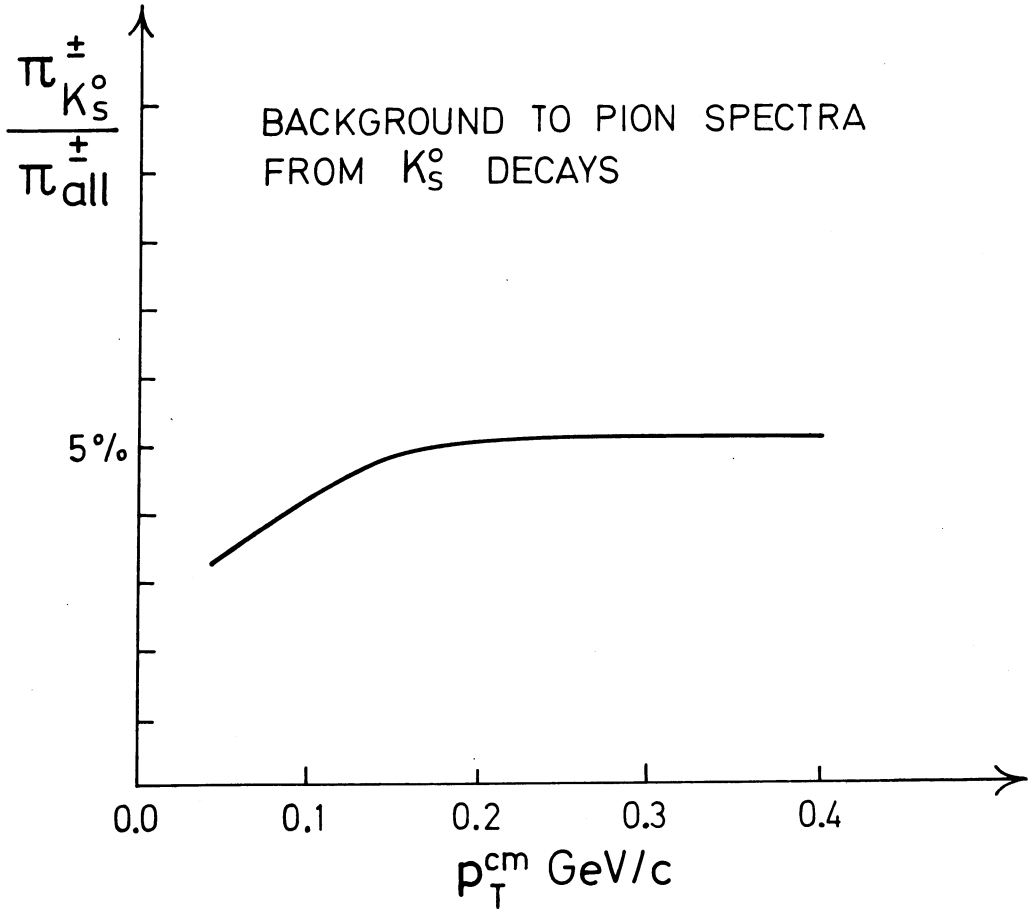
$\frac{\pi^{\pm}_{K^0_S}}{\pi^{\pm}_{all}}$
BACKGROUND TO PION SPECTRA
FROM K^0_S DECAYS
5%
0.0
0.1
0.2
0.3
0.4
p_T^{cm} GeV/c

Fig. 8

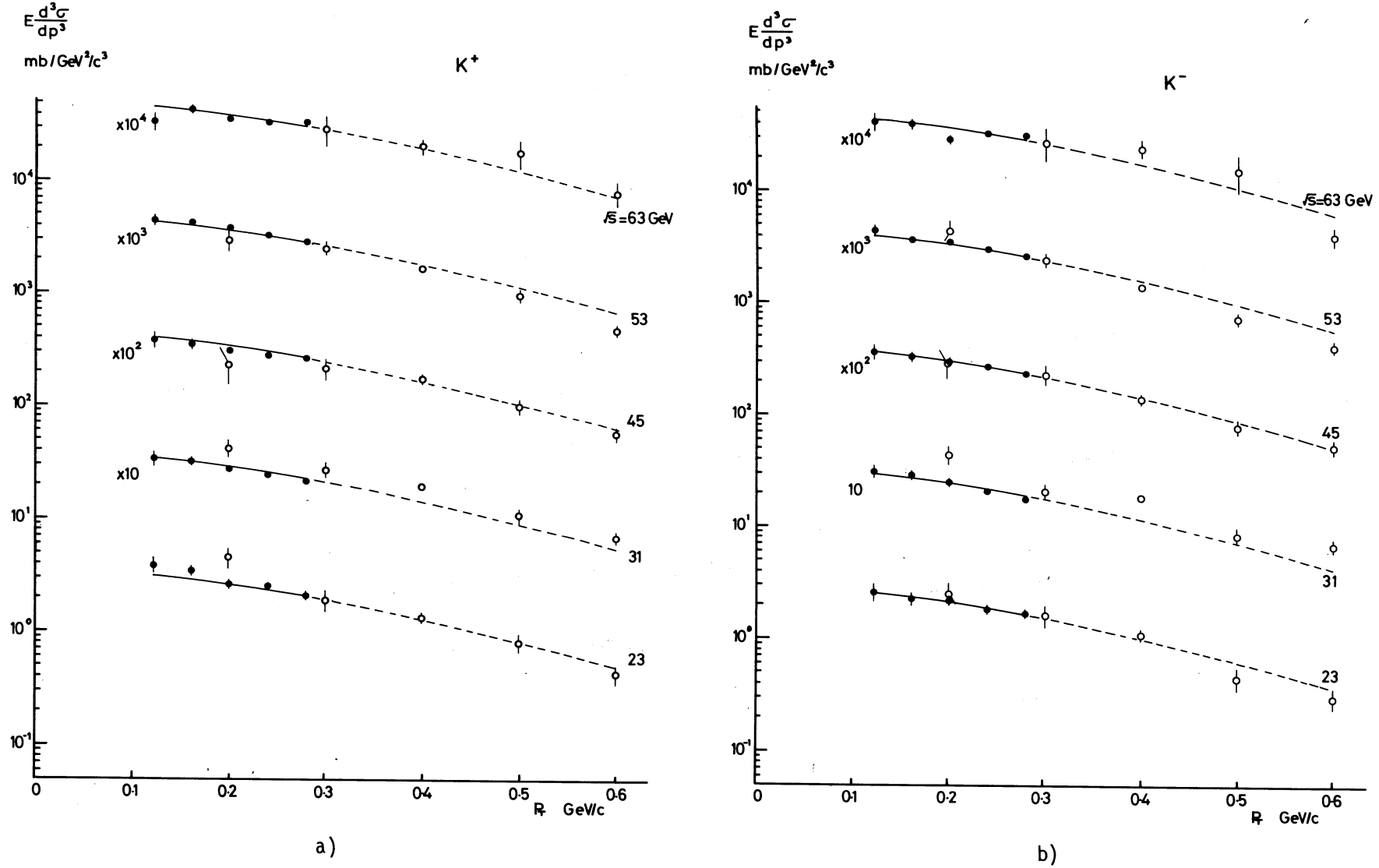
$E\frac{d^3\sigma}{dp^3}$
mb/GeV²/c³
K⁺
x10⁴
x10³
x10²
x10
√s=63 GeV
53
45
31
23
p GeV/c
a)
$E\frac{d^3\sigma}{dp^3}$
mb/GeV²/c³
K⁻
x10⁴
x10³
x10²
10
√s=63 GeV
53
45
31
23
p GeV/c
b)

Fig. 9

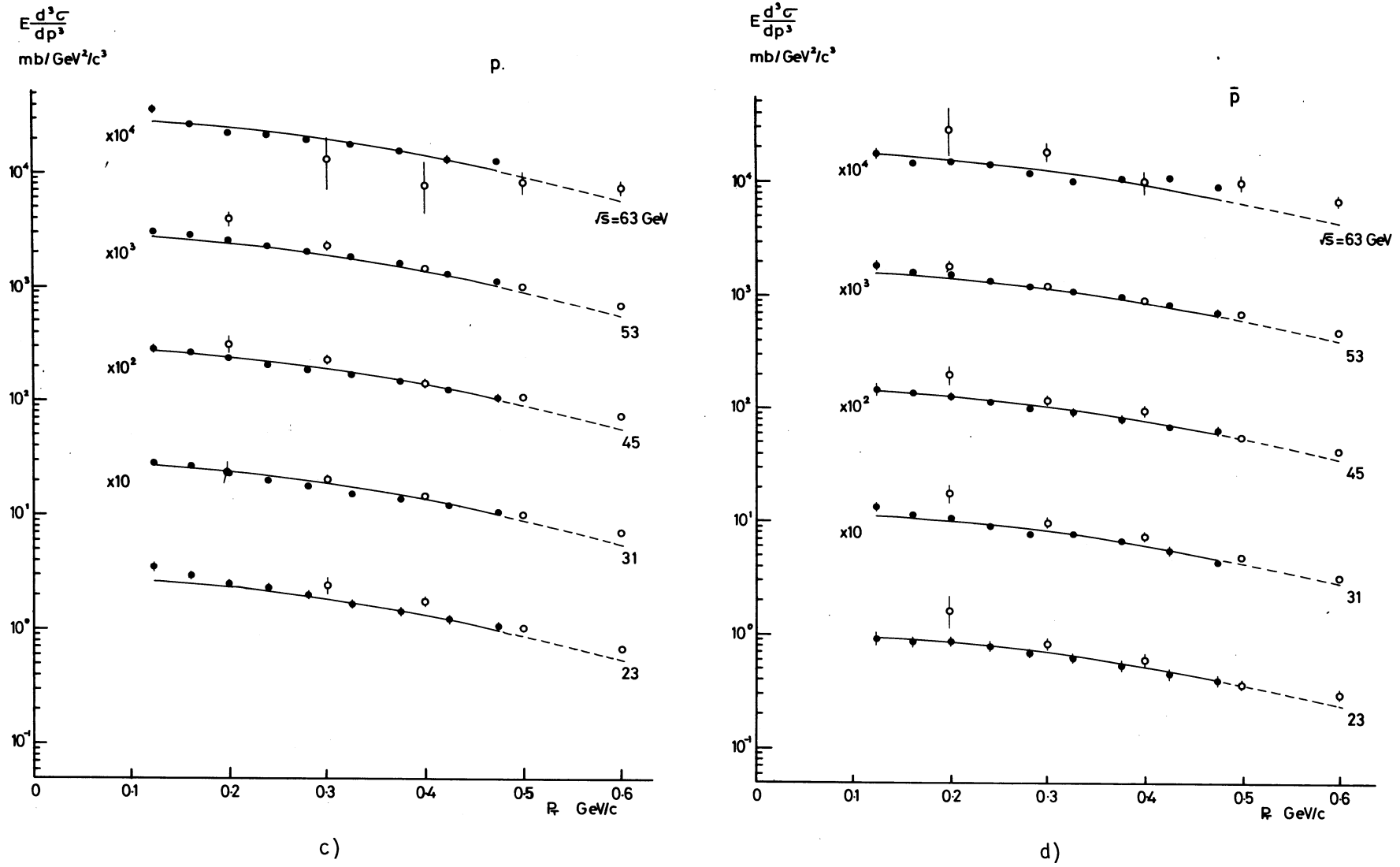
E d³σ/dp³
mb/GeV²/c³
p.
x10⁴
x10³
x10²
x10
√s=63 GeV
53
45
31
23
p_T GeV/c
c)
E d³σ/dp³
mb/GeV²/c³
p̄
x10⁴
x10³
x10²
x10
√s=63 GeV
53
45
31
23
p_T GeV/c
d)

Fig. 9

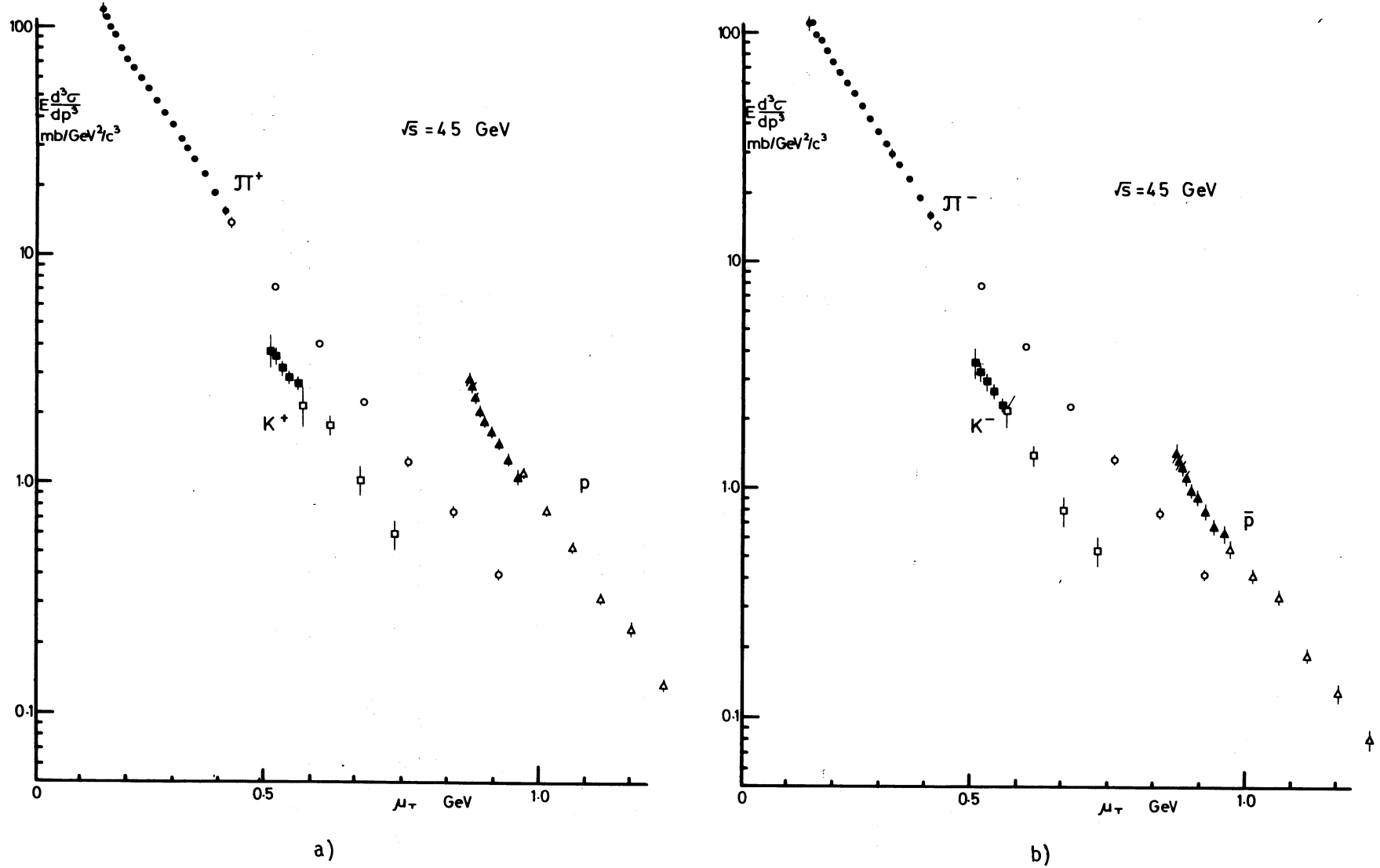
100
10
1·0
0·1
$E\frac{d^3\sigma}{dp^3}$
mb/GeV²/c³
√s = 4·5 GeV
π⁺
K⁺
p
0
0·5
1·0
μ_T GeV
a)
100
10
1·0
0·1
$E\frac{d^3\sigma}{dp^3}$
mb/GeV²/c³
√s = 4·5 GeV
π⁻
K⁻
p̄
0
0·5
1·0
μ_T GeV
b)

Fig. 10

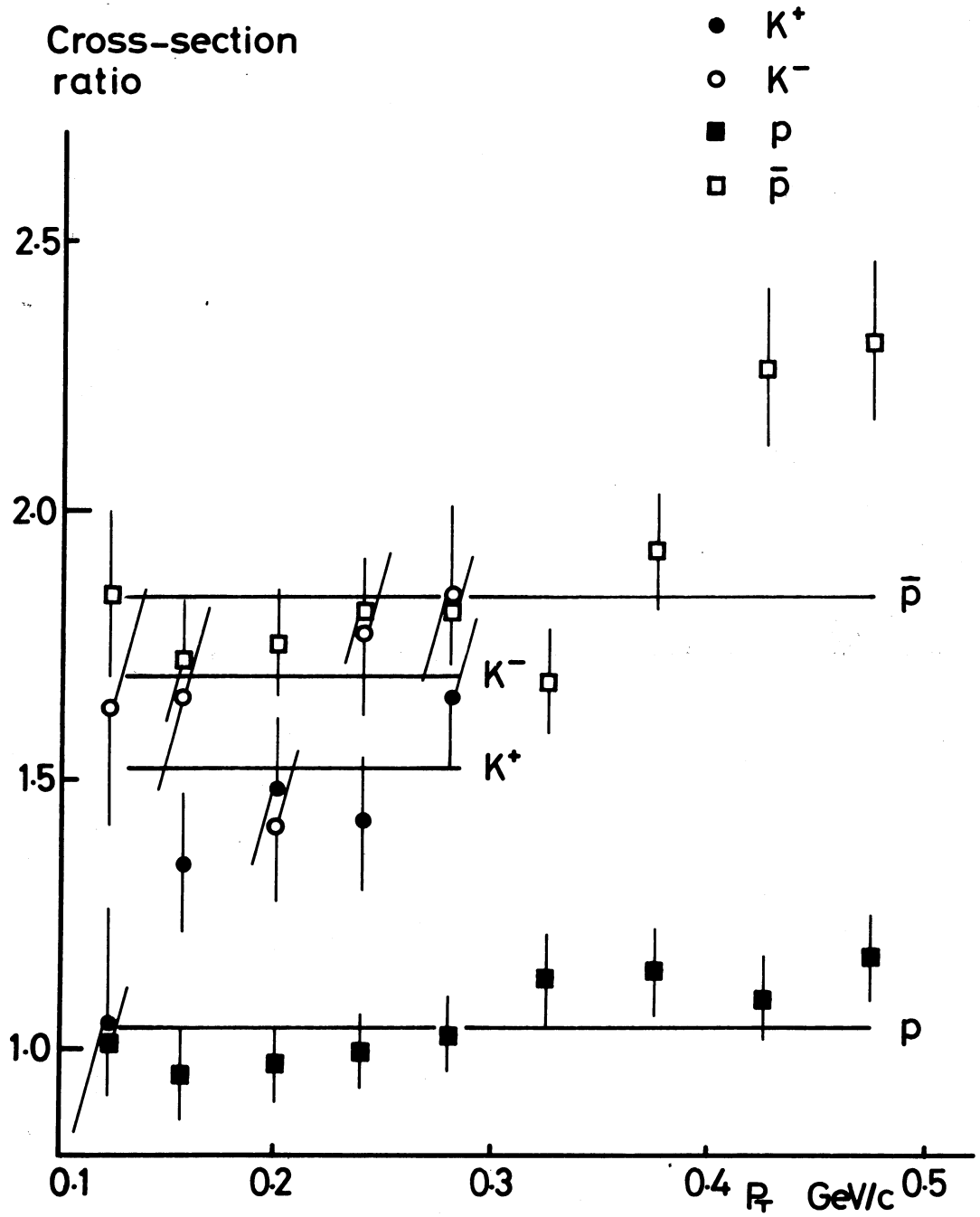

Fig. 11

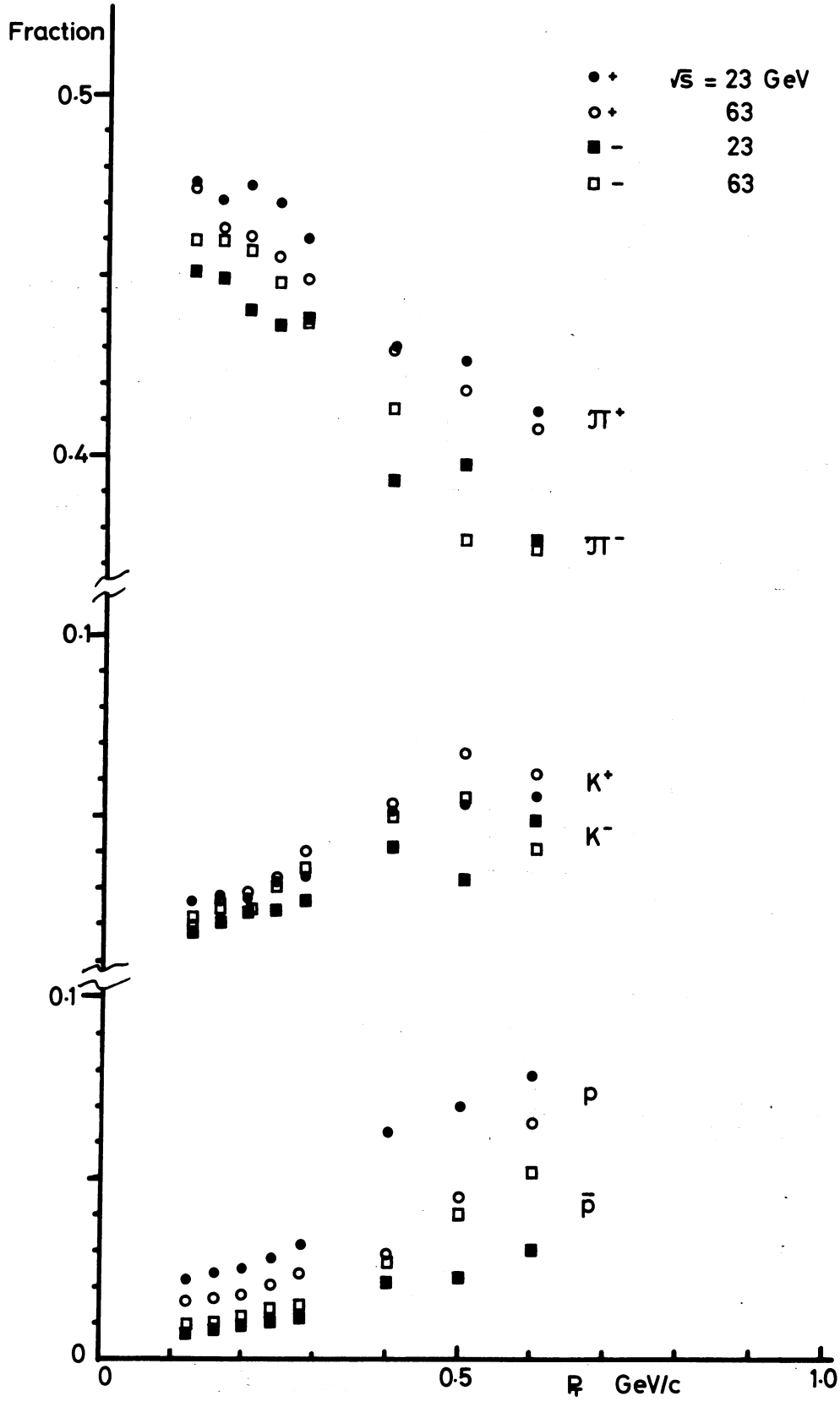

Fig. 12

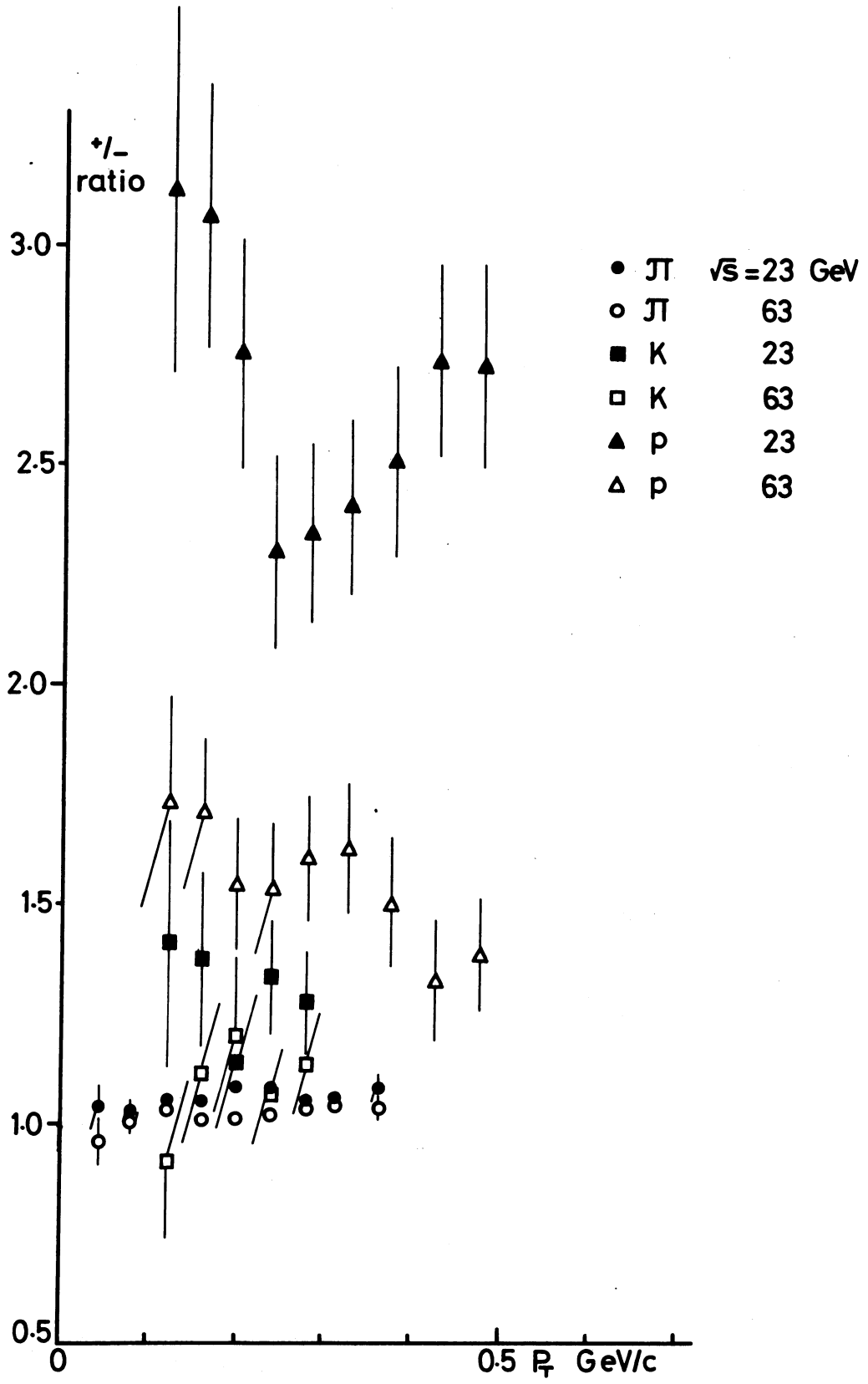

Fig. 13

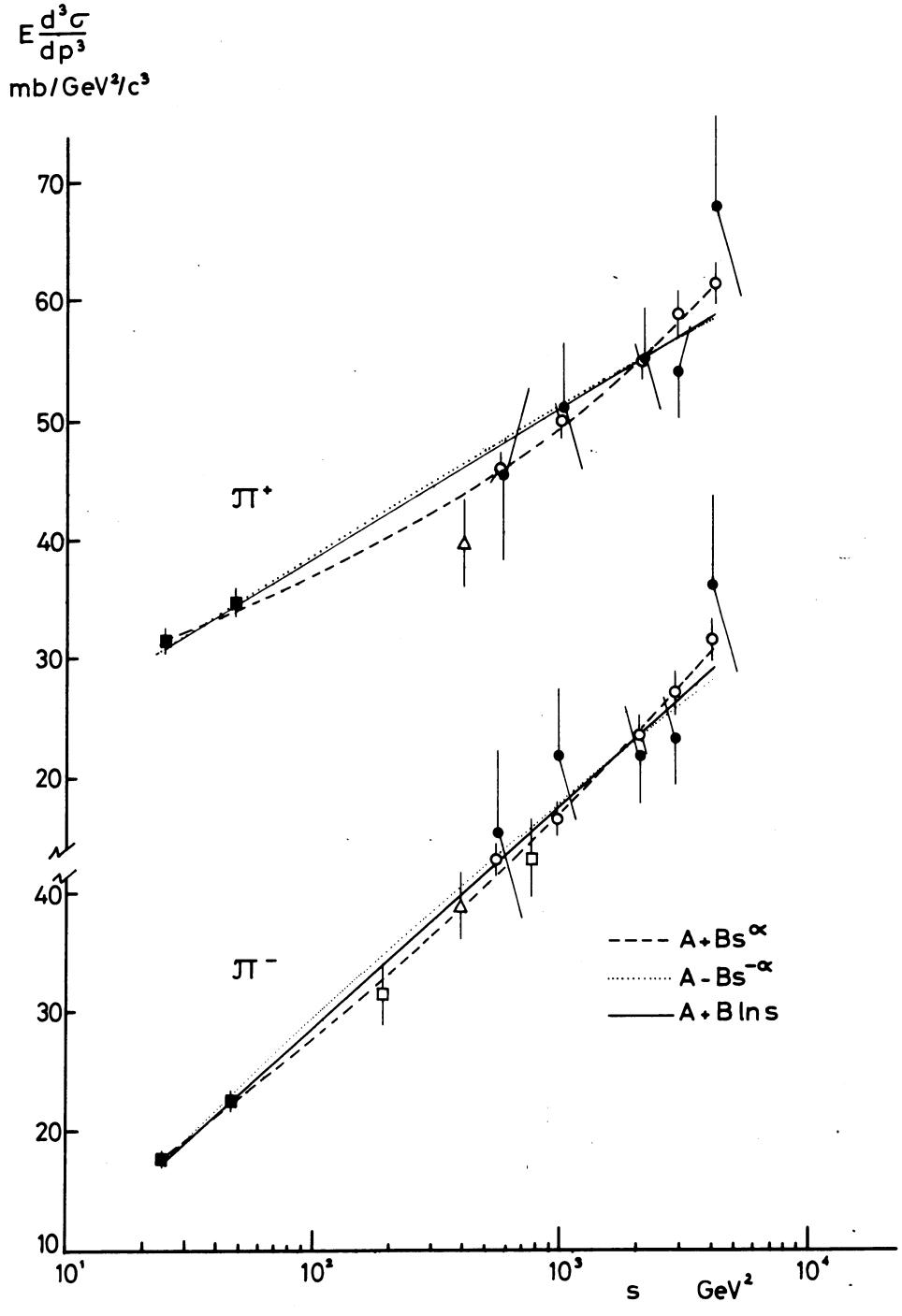
$E\frac{d^3\sigma}{dp^3}$
mb/GeV²/c³
70
60
50
40
30
20
40
30
20
10
π^+
π^-
$A+Bs^{\alpha}$
$A-Bs^{-\alpha}$
$A+B\ln s$
10^1
10^2
10^3
10^4
s GeV²

Fig. 14